Machine learning for the prediction of the local drag forces and heat transfer rates in turbulent flows past rough surfaces

Sanhueza, Rafael Diez; Akkerman, Ido; Peeters, Jurriaan W.R.

12th International Symposium on Turbulence and Shear Flow Phenomena (TSFP12)
Osaka, Japan (Online), July 19-22, 2022

MACHINE LEARNING FOR THE PREDICTION OF THE LOCAL DRAG FORCES AND HEAT TRANSFER RATES IN TURBULENT FLOWS PAST ROUGH SURFACES

Rafael Diez Sanhueza
Faculty of Mechanical, Materials and Maritime Engineering
Delft University of Technology
Leeghwaterstraat 39, 2628 CB, Delft, the Netherlands
R.G.DiezSanhueza-1@tudelft.nl

Ido Akkerman
Faculty of Mechanical, Materials and Maritime Engineering
Delft University of Technology
Mekelweg 2, 2628 CD, Delft, the Netherlands
I.Akkerman@tudelft.nl

Jurriaan W. R. Peeters
Faculty of Mechanical, Materials and Maritime Engineering
Delft University of Technology
Leeghwaterstraat 39, 2628 CB, Delft, the Netherlands
J.W.R.Peeters@tudelft.nl

ABSTRACT

Turbulent flows past rough surfaces can create substantial energy losses in engineering equipment. During the last decades, developing accurate correlations to predict the thermal and hydrodynamic behavior of rough surfaces has proven to be a difficult challenge. In this work, we develop a convolutional neural network architecture to perform a direct image-to-image translation between the height map of a rough surface and its detailed local drag resistance and heat transfer rates. Various techniques are discussed to improve the computational efficiency of the machine learning architecture proposed, and even to reduce its time and space complexity. The main study is based on a new DNS database formed by 24 flow cases at a friction Reynolds number of $Re_\tau = 180$ obtained by applying a random shift to the Fourier spectrum of the grit-blasted surface scanned by Busse *et al.* (2015,). The results show that machine learning can accurately predict the global values of the drag resistance and heat fluxes across a rough surface. The local predictions for both momentum and heat transfer also show a considerable improvement upon increasing the dataset size. A detailed analysis of the global skin friction values and Stanton numbers predicted by deep learning further reveals that the results surpass the accuracy of traditional correlations by a substantial margin in the dataset analyzed.

INTRODUCTION

Turbulent flows past rough surfaces can be found in a large variety of engineering applications. Irregular surfaces are often caused by external degradation processes, such as bio-fouling, abrasion, machining, or corrosion. The presence of rough surfaces can substantially increase the drag resistance of transportation systems, and lower the efficiency of thermodynamic cycles. One of the main challenges while working with rough surfaces is to predict the impact of a given surface topography on the drag resistance and heat transfer rates of a system. Most traditional correlations are based on standard surface metrics, such as the root-mean-squared height variations, skewness, kurtosis, effective slope, forward-facing angle, or different auto-correlation functions.

In this work, we develop a machine learning system based on convolutional neural networks to predict the local behaviour of turbulent flows past irregular surfaces. These systems are able to describe the complex physical effects observed when turbulent flows interact with rough walls. The complex non-linear functions required to approximate the behavior of turbulence are automatically reconstructed using a database containing rough surfaces with unique groups of topological features producing different flow effects.

DNS DATABASE

The study is based on a new DNS database formed by 24 flow cases at $Re_\tau = 180$. Numerical simulations are used instead of experimental measurements, since the local drag forces and heat fluxes correspond to quantities of interest. The flow cases are generated by applying a random phase shift to the Fourier spectrum obtained from the grit-blasted surface scanned by Busse *et al.* (2015,). The random shift is given by the variable ϕ_i in the following equation for the height function $H(x,z)$:

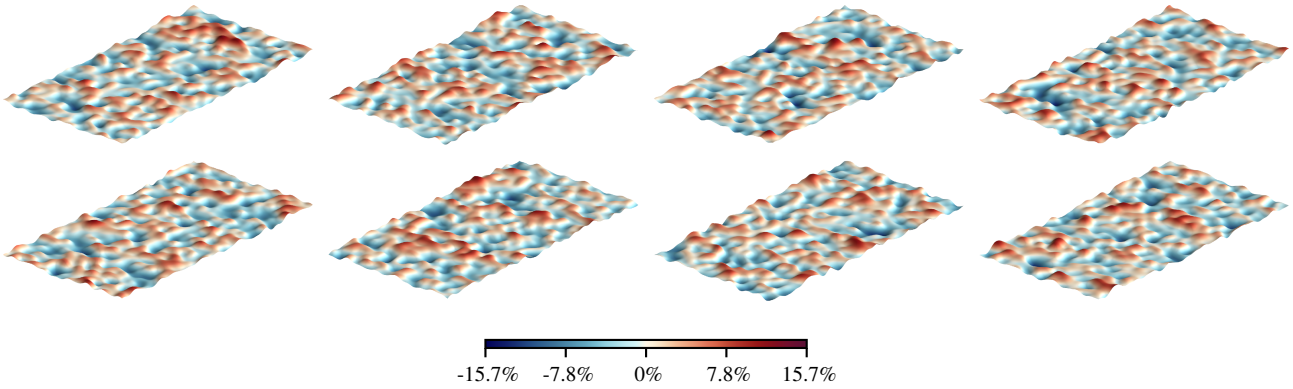

Figure 1. Examples of height maps generated by applying a random shift to the Fourier spectrum of the grit-blasted surface scanned by Busse *et al.* (2015,). All percentages are with respect to the half-channel height $\delta = L_y/2$.

$$H(x,z) = \sum_i R_i \cos\left(2\pi \left(M_i \frac{x}{L_x} + N_i \frac{z}{L_z}\right) - \phi_i\right) \quad (1)$$

The terms R_i, M_i, N_i correspond to constants extracted from the original Fourier spectrum for the grit-blasted surface. Figure 1 presents a collection of 8 examples with rough surfaces generated according to this technique. Despite the simplicity of the methodology used, every DNS case contains unique groups of topological features, which in turn create flow fields with different characteristics. Therefore, predicting the local drag forces and heat fluxes present in each DNS case corresponds to a challenging machine learning task.

The dimensionless Navier-Stokes equations and the energy equation solved for each DNS case are the following:

$$\nabla \cdot \mathbf{u} = 0, \quad (2)$$

$$\partial_t \mathbf{u} + \mathbf{u} \cdot \nabla \mathbf{u} = -\nabla p + Re_\tau^{-1} \nabla^2 \mathbf{u} + S_f, \quad (3)$$

$$\partial_t T + \mathbf{u} \cdot \nabla T = Pe_\tau^{-1} \nabla^2 T + S_q. \quad (4)$$

In eqs. (2-4), the variables $\mathbf{u}$, p, T correspond to the dimensionless velocity components, pressure and temperature respectively. The variable $Pe_\tau = Re_\tau Pr$ is the friction Peclet number, which is defined using the molecular Prandtl number Pr. The source terms S_f and S_q for the momentum and energy equations are equal to unity in all DNS simulations, as well as the Prandtl number $Pr = 1$. The velocity and temperature fields are scaled using the friction velocity $u_\tau = \sqrt{\tau_w/\rho}$ and the friction temperature $T_\tau = \dot{q}_w/(\rho c_p u_\tau)$. Since the reference density ρ and specific heat capacity c_p are equal to one, it can be further proven that $u_\tau = T_\tau = \dot{q}_w = 1$ for all the DNS cases considered. The numerical simulations are carried out using the in-house DNS code described by Peeters & Sandham (2019,). Identical discretization schemes are employed as in the original study. The friction Reynolds number (Re_τ) is set to 180. The domain size and the grid resolution have dimensions $(L_x \times L_y \times L_z) = (5.63 \times 2 \times 2.815)$ and $(N_x \times N_y \times N_z) = (280 \times 280 \times 140)$ in the streamwise, wall-normal and spanwise directions respectively. The scaling ratio for the height of the rough surfaces (k/δ) is kept at a constant value of 1/6, according to the definition of the original study.

In all the DNS cases generated, the bulk Reynolds numbers $Re_b = U_b L_y/\nu$ and the dimensionless bulk temperatures (T_b^+) presented nearly constant values of $Re_b = 4002$ and $T_b^+ = 11.21$ respectively. The maximum differences observed with respect to these quantities are 3.84% for Re_b and 2.82% for T_b^+. Therefore, all DNS cases employed similar mass fluxes and other bulk flow parameters. The velocity shifts observed in the log-layer (ΔU^+) for all DNS cases ranged from 4.09 to 5.07. The latter is equivalent to variations in the dimensionless Nikuradse sand-grain roughness height (k_s^+) from 24 to 33 according to the equations provided in the work of Thakkar *et al.* (2018,). Therefore, all DNS simulations contained similar levels of turbulence activity.

WALL FORCE INTERPOLATION

The local drag forces ($\mathbf{F}$) and heat transfer rates ($\dot{Q}$) acting over irregular surfaces are obtained by using a finite element integration scheme with face elements located at the rough walls. The equations integrated are the following:

$$\mathbf{F} = \iint_A \left(-P\,\mathbf{n} + \frac{1}{Re_\tau}\left(\nabla \mathbf{u} + \nabla \mathbf{u}^T\right) \cdot \mathbf{n}\right) dA, \quad (5)$$

$$\dot{Q} = \frac{1}{Pe_\tau} \iint_A \nabla T \cdot \mathbf{n}\, dA. \quad (6)$$

In eqs. (5-6), the variable A refers to the area of the rough surfaces in contact with the fluid. The vector $\mathbf{n}$ corresponds to the normal of the rough surfaces:

$$\mathbf{n} = \left(\sqrt{1 + \frac{\partial H}{\partial x}^2 + \frac{\partial H}{\partial z}^2}\right)^{-1} \left[-\frac{\partial H}{\partial x},\ 1,\ -\frac{\partial H}{\partial z}\right]^T. \quad (7)$$

The orientation of eq. (7) is intended to work with rough surfaces located at the bottom side of channel flows, where the wall-normal direction corresponds to the y-axis. For rough surfaces present at the top side of channel flows, the orientation of the vector $\mathbf{n}$ must be adjusted according to the transformations considered for the respective height function $H(x,z)$. The differential area dA for the rough surface elements is given by:

$$dA = \sqrt{1 + \frac{\partial H}{\partial x}^2 + \frac{\partial H}{\partial z}^2}\, dx\, dz. \quad (8)$$

After combining eqs. (5-8), it can be shown that the expression $\sqrt{1 + \partial H/\partial x^2 + \partial H/\partial z^2}$ cancels out. Therefore, if

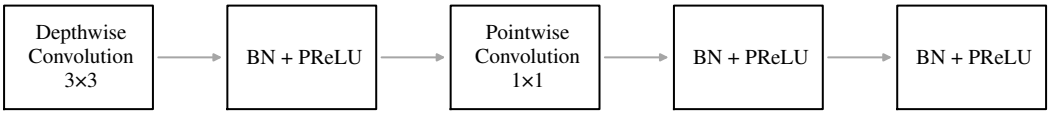

Figure 2. Schematic representation of the depthwise separable convolution (DSC) modules employed in the machine learning study. The abbreviation *BN* refers to the 2-D batch normalization operations applied before each PReLU activation function.

polynomial shape functions are used to represent the variables $(\mathbf{u}, P, T, H)$, then the final integrals given by eqs. (5-6) contain polynomial terms exclusively. Thus, a Gauss-Legendre integration scheme with a sufficient number of intermediate points can be used to find the analytical solution of the resulting integrals for the drag forces and heat fluxes.

In order to perform finite element integration, the variables $(\mathbf{u}, P, T, H)$ were reconstructed using shape functions based on a symmetric stencil of data points surrounding each finite element. The degree of the polynomial terms chosen in each direction can be found in Table 1. Here, it can be noted that all interpolation schemes considered linear terms in the wall-normal direction (y), whereas mixed-order linear or quadratic terms were considered in the horizontal directions ($x-z$). The latter was necessary because the DNS solver employed a staggered discretization scheme to handle the velocity components $\mathbf{u} = (u_x, u_y, u_z)$. Therefore, the number of data points required to form a symmetric stencil was different in each direction. The usage of linear interpolation schemes in the wall-normal direction was validated empirically, since it was noted that quadratic terms yielded slightly higher errors with respect to both the global force and heat transfer balances. All FEM integration areas considered for eqs. (5-6) were centered around the original $x-z$ coordinates for the pressure and temperature fields (P, T). The pressure field was extrapolated in the wall-normal direction (y) by considering the first two data points available above the rough surfaces. However, the velocity and temperature fields $(\mathbf{u}, T)$ considered that the first layer of data points was located exactly over the rough surfaces at the corresponding $H(x,z)$ locations, with a value equal to the homogeneous boundary conditions ($\mathbf{u} = T = 0$).

The final numerical implementation was written in PyTorch, since it can be proven that the entire numerical procedure can be expressed as a sequence of parallelizable array operations. The process of gathering data points located in neighboring $x-z$ locations can be expressed using standard array shift operations due to the presence of periodic boundary conditions for the rough surfaces. The linear systems of equations required to fit separate shape functions for the flow variables (u_x, u_y, u_z, P, T) surrounding each FEM integration area can be solved using 4-D tensors containing batches with small systems of equations.

MACHINE LEARNING

In order to predict the local drag forces (f_x) and heat fluxes $(\dot{q})$ acting over irregular surfaces, it is necessary to build advanced non-linear models based on techniques such as machine learning. A preliminary assessment revealed that linear regression models presented a low degree of correlation between the input height map $H(x,z)$ for a DNS case and the observed ground-truth data for $f_x(x,z)$ or $\dot{q}(x,z)$. The average L1-errors with respect to the total drag forces and heat transfer rates reached magnitudes up to 114% and 42.2% using linear models respectively. Therefore, it was decided to build predictive systems based on convolutional neural networks to scan the input height maps $H(x,z)$ of the rough surfaces.

Table 1. Order of the polynomial terms considered by the shape functions in every direction.

Variable	Streamwise (x)	Vertical (y)	Spanwise (z)
P	2	1	2
T	2	1	2
u_x	1	1	2
u_y	2	1	2
u_z	2	1	1
H	2	-	2

The final machine learning study is based on a deep learning architecture formed by depthwise separable convolution modules (Chollet, 2017). The overall shape of the ML architecture is presented in Table 2, whereas the details of each convolution module are described in Figure 2. Every module has an internal dimension of 20 channels, 3×3 depthwise convolutions, and three PReLU activation functions (He *et al.*, 2015) preceded by batch normalization. The usage of ReLU operators is avoided during the machine learning study, since PReLU neurons increase the expressivity of neural networks with a minimal computational cost, and they can facilitate the convergence of the training procedure. Max-pooling operators are also avoided because they lose the exact spatial location of the features being processed. Every machine learning model created has a total of 5,780 trainable parameters.

The training procedure for each machine learning configuration is driven by L1 loss functions instead of traditional L2 metrics. This choice helps the optimizer to train models that focus on predicting the global values for the drag forces and heat transfer rates with greater precision than L2 loss functions, which tend to over-penalize small regions with outlier points. Physics-informed data augmentation is performed by mirroring all DNS cases with respect to the spanwise axis. The final study is based on the leave-one-out cross-validation technique, which is beneficial for small datasets (Wong, 2015).

The overall time and space complexity of the machine learning system can be substantially improved by creating a direct image-to-image translation system between the input height map $H(x,z)$ for a DNS case and the output predictions for the local drag forces $f_x(x,z)$ or heat transfer rates $\dot{q}(x,z)$. A schematic representation of this approach can be found in Figure 3. Here, it can be noted that the standard convolutional neural network shown in Figure (3.a) systematically reduces an input image until a single output prediction is obtained for $f_x(x,z)$ or $\dot{q}(x,z)$, discarding all intermediate information. This approach is highly inefficient while generating predictions for

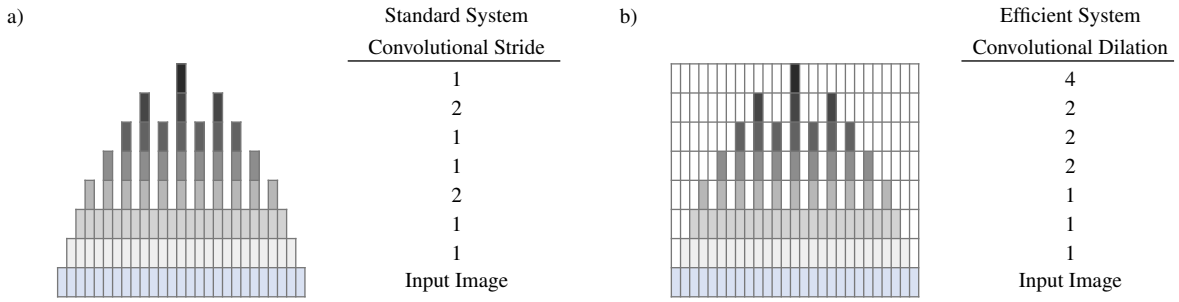

Figure 3. Comparison in 1-D between a standard convolutional neural network and the efficient computer vision system developed.

neighboring (x,z) spatial locations sharing a large number of input pixels in their local height maps, since the same convolutional operations must be repeated again. In contrast, the advanced computer vision system shown in Figure (3.b) avoids redundant operations, since the results of intermediate convolutional layers are computed only once, and the upcoming layers share information by utilizing a modified dilation system that produces the same effect as applying reduction strides in a traditional convolutional neural network. As a result, an array with all output predictions for $f_x(x,z)$ or $\dot{q}(x,z)$ for a DNS case is computed after only one pass through the neural network. The empty rectangles shown in Figure (3.b) correspond to information that is not connected to the output prediction highlighted at the top, but is used to process other neighboring data points. In terms of computational efficiency, the approach shown in Figure (3.b) is able to reduce the baseline time complexity required to process an input height map $H(x,z)$ discretized as an image with N pixels from quadratic time $\mathcal{O}(N^2)$ to linear time $\mathcal{O}(N)$. Therefore, the running times using the approach described in Figure (3.b) are orders of magnitude lower than traditional computer vision architectures, which process one image for every data point predicted. Moreover, the methodology described in Figure (3.b) can also reduce the space complexity and RAM memory requirements of the machine learning system during both the training and evaluation stages, since only one image is processed per DNS case. Finally, circular padding is applied to the convolutional architecture presented in Figure (3.b) to account for the periodic boundary conditions considered for the rough surfaces.

Table 2. Layers present in the deep learning architecture. The columns C_{in}, C_{out}, D and $AF\&B$ refer to the number of input channels, output channels, dilation and the presence of activation functions with bias respectively. The column *Input Image* refers to the equivalent input image size considered by each convolutional layer, with respect to a total image size of 280×140 for the entire DNS domain. The final layer Conv. 2D corresponds to a simple convolutional filter with a kernel size of 3×3. The architecture of the *DSC* modules is presented in Figure 2.

Layer	C_{in}	C_{out}	D	$AF\&B$	Input Image
DSC	1	20	1	Yes	119×61
DSC	20	20	2×1	Yes	59×59
DSC	20	20	4×2	Yes	29×29
DSC	20	20	4×2	Yes	27×27
DSC	20	20	8×4	Yes	13×13
DSC	20	20	8×4	Yes	11×11
DSC	20	20	16×8	Yes	5×5
Conv. 2D	20	1	16×8	-	3×3

RESULTS

The results of the machine learning study can be found in Figures 4 and 5. In Figure 4, a comparison is presented between the local drag forces and the heat fluxes obtained by the deep learning system with respect to the original DNS data. As it can be seen in Figure 4, the machine learning predictions show physically realistic trends, with the majority of the errors located in areas where large spatial variations in the local drag forces or heat transfer rates are expected. A detailed analysis of the global errors obtained for the force and heat transfer balances revealed that most of the errors were lower than 5% during the cross-validation study, whereas the maximum errors recorded were 13.21% for the drag forces and 5.99% for the heat fluxes. Both of these results can be regarded as satisfactory. Figure 5 presents histograms comparing the distributions of the local errors obtained using datasets with 7, 12 and 24 DNS samples. These results reveal that the errors obtained for the momentum and heat transfer predictions present a substantial improvement upon increasing the dataset size from 7 to 24 DNS samples. The predictions using 12 DNS cases show mixed trends, since the errors for the local drag forces are similar to the study using 24 DNS cases, yet the errors for the local heat fluxes only present moderate improvements. The relatively large errors obtained for the momentum predictions, compared to the heat fluxes, are partially caused by the fact that the local drag forces reach magnitudes up to 23 times larger than the average values for the DNS data, whereas the largest heat fluxes only reach values up to 8.1 times higher. Therefore, minor differences in areas where strong drag forces are expected will create much greater errors than similar percentual differences in regions where large heat fluxes occur.

In Figure 4, the streamwise patterns observed in the errors for the heat fluxes are likely caused by the reduced scope of the input images considered to perform predictions. While it is ideal from a physical perspective to build a predictive systems considering the largest input images available, the usage of images with more pixels can lead to neural networks with an increased number of parameters, and the associated risk of over-fitting. Therefore, a trade-off must be considered between the size of the input images, and the increased number of parameters that the neural network will require to process more

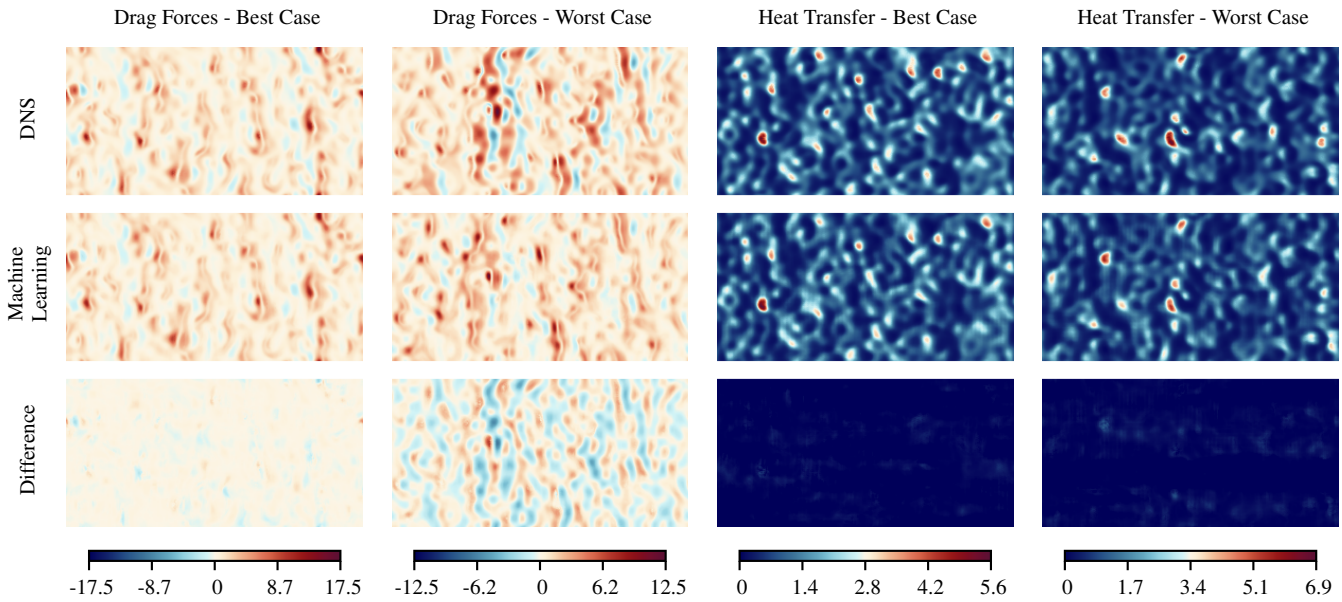

Figure 4. Comparison between the local drag forces and heat transfer predictions obtained by the deep learning system with respect to the DNS data. The cases presented were selected based on the highest and the lowest values for the L1-norm of the local errors. The values of each colormap indicate the ratio between the local quantities and the average drag forces or heat fluxes present in the DNS data.

input pixels. The influence of the input images becomes more evident for the heat transfer predictions than for momentum, since the higher accuracy of the deep learning system implies that the assumptions established during the modelling process start to become noticeable. Another important insight is that the results obtained during the worst-case scenario for the momentum predictions originated from a rough surface which had yielded favorable results while using 12 DNS samples instead of 24 cases. Therefore, it can be concluded that the momentum predictions present signs of over-fitting, and that further research is required to determine if the errors can be reduced by incorporating more training data, or if the architecture of the deep learning model can be further optimized.

After obtaining the deep learning predictions, a study was conducted to analyze the trends observed for the skin friction factors (C_f) and the Stanton numbers (St). Among the traditional correlations proposed in the literature to predict the skin frictions factors (C_f) or the equivalent Nikuradse sand-grain roughness ($k_{s,eq}$), it was determined that the correlation developed by Flack & Schultz (2010,) yielded accurate predictions:

$$k_{s,eq} = 4.43\ S_q\ (1 + S_{sk})^{1.37}. \tag{9}$$

In eq. (9), the variables S_q and S_{sk} correspond to the root-mean squared height variations and the surface skewness respectively. A detailed review of the numerical procedure to calculate these variables can be found in the work of Thakkar *et al.* (2017,). The system of equations to calculate the skin friction factor (C_f) is completed using the formulas described by Peeters & Sandham (2019,), and the non-linear function $\Delta(U^+) = f(ks^+)$ provided by Thakkar *et al.* (2018,). The values for the Stanton number (St) are obtained by applying the correlation proposed by Dipprey & Sabersky (1963,). These equations establish a methodology to predict the Stanton number (St) of a rough surface based on a skin friction factor (C_f) previously calculated. In Figure 6, the histograms present the errors obtained for C_f and St based on the deep learning predictions and the traditional formulas previously described, which are based on the work of Flack & Schultz (2010,) and Dipprey & Sabersky (1963,). As it can be seen in the subfigures, the deep learning system is substantially more accurate than traditional correlations while predicting both momentum (C_f) and heat transfer (St) parameters. The maximum errors for the skin friction coefficients C_f in the deep learning system reached values of 13.21%, whereas the system with traditional correlations reached values up to 15.61%. Therefore, it can be concluded that deep learning constitutes a valid alternative to generate improved predictions for flow parameters, such as C_f or St, if enough training data is collected.

CONCLUSION

This study presented a deep learning architecture capable of predicting detailed maps for the local drag forces and heat fluxes acting over irregular surfaces. The results show that machine learning is able to achieve reliable results while predicting the global force and heat transfer balances. A sensitivity study with respect to the dataset size also revealed a significant reduction in the errors for the momentum and heat transfer predictions once the dataset size is increased from 7 to 24 DNS cases. The comparisons performed with respect to traditional correlations proved that deep learning is a valid alternative to generate improved predictions for important flow parameters, such as the skin friction factors (C_f) or the Stanton number (St). Therefore, it is recommended to perform further research regarding the creation deep learning models to predict the behavior of turbulent flows past rough surfaces.

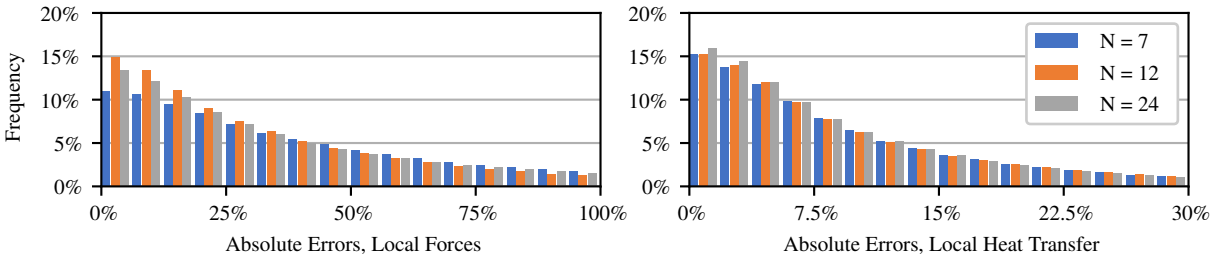

Figure 5. Changes in the distribution of the absolute errors for the momentum and heat transfer predictions with respect to the dataset size. All errors are scaled using the average DNS values for the drag forces or heat transfer rates.

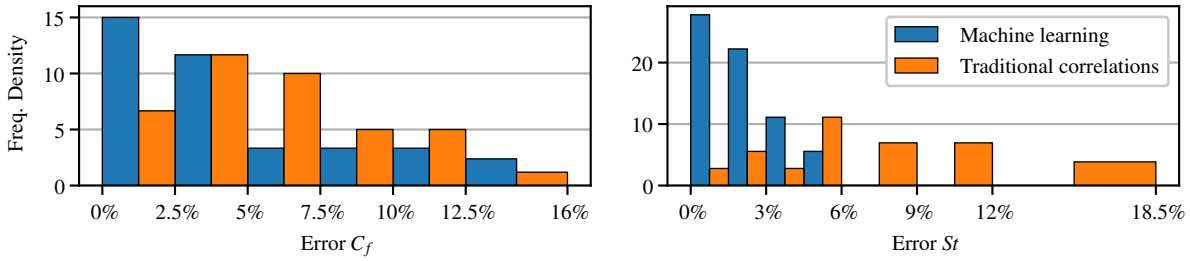

Figure 6. Histograms comparing the distribution of errors for the skin friction values C_f and the Stanton numbers St between the deep learning model and the traditional correlations of Flack & Schultz (2010,) and Dipprey & Sabersky (1963,).

REFERENCES

Busse, A., Lützner, M. & Sandham, N. D. 2015, Direct numerical simulation of turbulent flow over a rough surface based on a surface scan. *Computers & Fluids* **116**, 129–147.

Chollet, F. 2017, Xception: Deep learning with depthwise separable convolutions. In *IEEE Conference on Computer Vision and Pattern Recognition*, pp. 1800–1807.

Dipprey, D.F. & Sabersky, R.H. 1963, Heat and momentum transfer in smooth and rough tubes at various prandtl numbers. *International Journal of Heat and Mass Transfer* **6** (5), 329–353.

Flack, Karen A. & Schultz, Michael P. 2010, Review of Hydraulic Roughness Scales in the Fully Rough Regime. *Journal of Fluids Engineering* **132** (4), 041203.

He, K., Zhang, X., Ren, S. & Sun, J. 2015, Delving deep into rectifiers: Surpassing human-level performance on imagenet classification. In *IEEE International Conference on Computer Vision*, pp. 1026–1034.

Peeters, J.W.R. & Sandham, N.D. 2019, Turbulent heat transfer in channels with irregular roughness. *International Journal of Heat and Mass Transfer* **138**, 454–467.

Thakkar, Manan, Busse, Angela & Sandham, Neil 2017, Surface correlations of hydrodynamic drag for transitionally rough engineering surfaces. *Journal of Turbulence* **18** (2), 138–169.

Thakkar, M., Busse, Angela & Sandham, Neil 2018, Direct numerical simulation of turbulent channel flow over a surrogate for nikuradse-type roughness. *Journal of Fluid Mechanics* **837**.

Wong, Tzu-Tsung 2015, Performance evaluation of classification algorithms by k-fold and leave-one-out cross validation. *Pattern Recognition* **48** (9), 2839–2846.